Faraday waves in a circular tank

Stuart William Colville[a], **Y.-M. Scolan**[b], Francesco Gambioli[c], Yeaw Chu Lee[a], Deborah Greaves[a], Edward Ransley[a]
a. University of Plymouth (UK)
b. ENSTA-Bretagne (France)
c. Airbus, Pegasus House (UK)
Email: stuart.colville@plymouth.ac.uk

1 Introduction

The present abstract is concerned with highly nonlinear free surface deformation in a circular tank. This simplified tank is the cross section of a horizontal cylinder which aims at carrying liquefied hydrogen (LH_2) in aircraft (see Colville et al. (2023)). The problem is considered quasi two-dimensional, hence it is greatly simplified compared to the actual configuration. Furthermore we focus on the motion of the interface when the tank has forced vertical oscillating motion only; the vertical direction corresponding to the direction of the acceleration of gravity, this condition is known to yield Faraday waves. In aircraft vertical accelerations can occur in turbulence, dynamic landing and taxiing. The theoretical evidence of Faraday waves in a circular tank is first investigated in linear potential theory. The experimental set-up and results are shown thereafter, and compared to derived eigenfrequencies.

2 Faraday waves in linearized potential theory

We consider the nonlinear boundary conditions along the interface between two fluids with arbitrary density ratio, $r = \rho_g/\rho_f$ where the indices $_f$ and $_g$ refer to the variables attached, the heavier fluid (liquid) and the lighter fluid (gas) respectively. The two fluids are immiscible and their kinematics are described in potential theory. At the instantaneous interface of the two fluids, we impose the continuity of the pressure and the normal velocities.

$$\phi_{f,t} + \frac{1}{2}(\vec{\nabla}\phi_f)^2 + G(t)y = r\left(\phi_{g,t} + \frac{1}{2}(\vec{\nabla}\phi_g)^2 + G(t)y\right), \quad \vec{\nabla}\phi_f \cdot \vec{n} = \vec{\nabla}\phi_g \cdot \vec{n}, \tag{1}$$

where ϕ_f and ϕ_g describes the fluid motion in the coordinate system attached to the tank and the total vertical acceleration $G(t) = g + \gamma \cos \Omega t$ contains the gravity g and the oscillating forced vertical acceleration of the tank.

The Faraday waves are sought after the linearization of the boundary value problem is performed. In order to calculate the velocity potentials in both phases, we adopt the method of solution exposed in McIver (1989) for a single phase and further developed for two phases in Scolan (2015). To this end, a conformal mapping of the inner circular tank (radius $D/2$) is performed, $x + iy = ih - e \tanh\left(\frac{\alpha+i\beta}{2}\right)$; h is the filling measured from the south pole and e is the length of the interface. The two lines $\beta = \beta_f$ and $\beta = \beta_g$ are the images of the circular arcs wetted by the fluids f and g respectively. The interface corresponds to $\beta = 0$. In the transformed plane, the linear solution in phase f reads

$$\phi_f(\alpha, \beta, t) = \int_0^\infty \frac{D_{,t}(\tau, t)}{\sqrt{\tau f(\tau) \sinh \tau\beta_f \cosh \tau\beta_f}} \cosh \tau(\beta - \beta_f) m(\tau\alpha) d\tau, \quad f(\tau) = 1 - r\frac{\tanh \tau\beta_f}{\tanh \tau\beta_g} \tag{2}$$

where the function m is either sin or cos functions depending on the antisymmetric or symmetric interface deformation respectively. Then the combination of the linearized kinematic and dynamic boundary conditions at the interface gives

$$(1 - r)G(t)D(\tau', t) = -e\int_0^\infty D_{,t^2}(\tau, t)K(\tau, \tau')d\tau, \quad \tau' \in [0, \infty[\tag{3}$$

where the operator K is detailed in Scolan (2015). By using the change of variable $u = 2e^{-\tau} - 1$, the interval of integration is turned into $[-1 : 1]$. Then the integral equation (3) is discretized with a Gauss-Legendre quadrature scheme, yielding an equivalent linear system

$$eKD_{,t^2} + (1 - r)G(t)D = 0 \tag{4}$$

where K is a known square matrix and D is now a vector that depends on time only. The matrix K can be written $K = PHP^{-1}$ where H is a diagonal matrix containing the eigenvalues of K and the columns of P are the eigenvectors of K. As a consequence equation (4) is written for a vector $E = P^{-1}D$

$$eHE_{,t^2} + (1 - r)G(t)E = 0 \tag{5}$$

This is an uncoupled system of well known Mathieu equations for each component of the vector E. The standard stability analysis is performed. Provided that no damping acts on the dynamical system, and by noting ω_2 the first symmetric eigenfrequency of the unforced system ($\gamma = 0$) it is well known that the first limit of stability occurs when the ratio of frequencies is $\Omega = 2\omega_2$. This result is also shown in Kumar & Tuckerman (1994) but for another two fluid system (infinite horizontal strips). Fig. 1a shows the variation of the first mode antisymmetric and symmetric nondimensional eigenfrequency $D\omega_1^2/2g$ and $D\omega_2^2/2g$ with the filling ratio h/D. Fig. 1b shows the variation of first mode symmetric nondimensional eigenfrequencies $D\omega_2^2/2g$ in terms of the density ratio r. The eigenfrequency where $\rho_{air}/\rho_{water} = 0.0012$ is displayed in Fig. 1b, at small density ratio's there is little change in the eigenfrequency from ρ_{air}/ρ_{water}=0. This eigenfrequency is compared with experimental results in the following section with the two fluids water and air in the steady state under forced excitation.

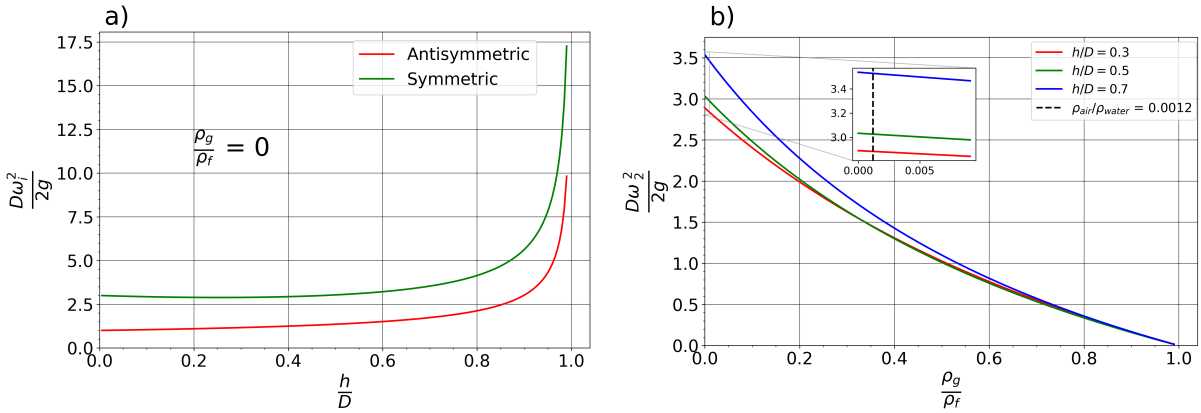

Figure 1: a) Non dimensional eigenfrequency first mode b) variation of first symmetric mode in terms of density ratio

3 Experimental setup and illustrative results

The experimental campaign investigates Faraday waves at the fundamental symmetric mode. The experimental setup, Fig. 2a, is similar to the one described in Colville et al. (2023). In this case the frame is mounted vertically and the tank is excited vertically. This parametric study varies the forcing amplitude, forcing frequency and fluid fill level. Spatial and temporal surface profiles of the fluid free surface, in the steady state are obtained using a high-speed camera (HSC). Images are acquired at 60 frames per second (fps) with a shutter speed of 1/12000s-1/15000s and spatial resolution 1024x1024 pixels. Two high intensity lights are positioned at the edge of the tank, their light is reflected and diffused off a white background screen directly behind the tank, this lighting setup has been employed previously (see Gambioli et al. (2019)).

An image processing algorithm (IPA) extracts the free surface profile from the HSC images (Fig. 2b). The IPA identifies the moving region of interest for every frame. The Canny edge detection method (see Canny (1986)) is utilised on the region of interest and the fluid free surface co-ordinates are extracted. The free surface position is converted to world co-ordinates using the known diameter of the tank and the detected circle diameter - in pixel co-ordinates. Three free surface points are extracted, the left and right sidewalls (LS and RS) and the free surface centre (FSC). The steady state sloshing amplitude (half of the peak to trough displacement) for each of the extracted free surface points is then obtained for every test case.

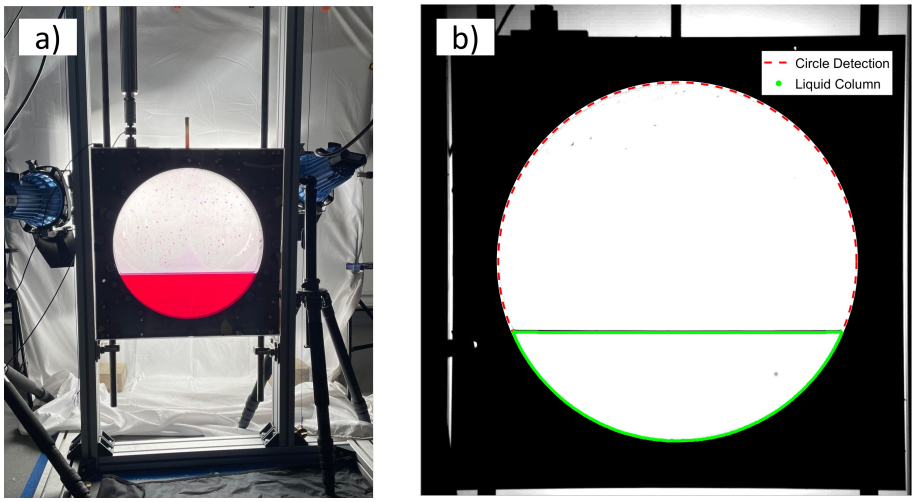

Figure 2: a) Experimental setup b) Static free surface overlaid on original image

Fig. 3 shows the steady state sloshing amplitude (A_0/D) against the frequency ratio ($\Omega/2\omega_2$). The fill level ($h/D = 0.3$) is presented in Fig. 3a for three different driving amplitude's. This shows that as the driving amplitude is increased, the sloshing amplitude increases. The maximum sloshing amplitude occurs below the theoretical liquid natural frequency for all forced amplitudes tested. This is characteristic of a soft spring nonlinear response. This nonlinearity increases as the forced amplitude is increased, this is displayed on Fig. 3a as the maximum sloshing amplitude occurs further from the theoretical eigenfrequency. Generally, symmetry is observed between the left and right sidewall displacements. The largest free surface displacement occurs at the left and right sidewall with the free surface centre showing consistently smaller displacements. At greater sloshing amplitudes the difference between respective sidewalls and the free surface centre increases. Fig. 3b

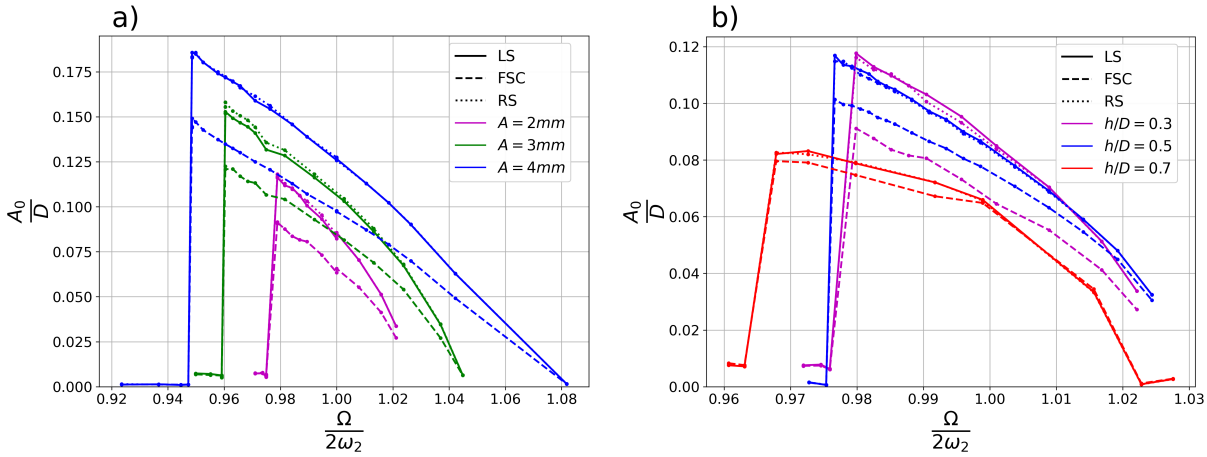

Figure 3: a) 0.3 fill level fluid response with varying driving amplitude b) Fluid response for varying fill level at constant driving amplitude

displays a comparison of different fill levels where the driving amplitude is kept constant ($A = 2mm$). The 0.7 fill level shows the smallest sloshing amplitude at resonance and the greatest nonlinearity - $\Omega/2\omega_2$ shifted further below one. The 0.3 fill level exhibits the highest sloshing amplitude at resonance and the closest resonant frequency to theory. The fill level clearly affects the degree of nonlinearity in fluid response. There is greater nonlinearity at greater fill levels. Fig. 3b shows that the fill level effects the difference in sloshing amplitude between the antinodes (symmetric sidewalls and the FSC). The largest difference in magnitude occurs where $h/D = 0.3$ and the smallest difference in magnitude occurs at the 0.7 fill level.

Fig. 4 shows the maximum sloshing amplitude case tested for a 0.3 fill level. Spatial profiles of the free surface across a temporal cycle are displayed. Fig. 4a shows the increasing wave elevation where

$t_{trough} < t < t_{peak}$. Fig. 4b shows the subsequent decreasing wave elevation $t_{peak} < t < t_{trough}$. Fig. 4a shows the maximum wave steepness at t=0.27s, the wave velocity at this point is zero. Following this, Fig. 4b shows the wave elevation descending from t=0.30s - t=0.50s. The overall mode shape displays asymmetries between the wave elevation ascending and the wave elevation descending.

It was observed during the experimental campaign, where $h/D = 0.3$, that if the driving amplitude is further increased, wave breaking occurs at the FSC crest and droplets are ejected from the liquid column. It was also observed experimentally, for the 0.7 fill level, that wave breaking occurs at the tank sidewalls at small driving amplitudes ($\geq 3mm$) near resonance. Therefore, the liquid column maintains its structure (no breaking) for larger driving amplitudes at lower fill levels. This leads to greater wave steepness values at lower fill levels (with no wave breaking).

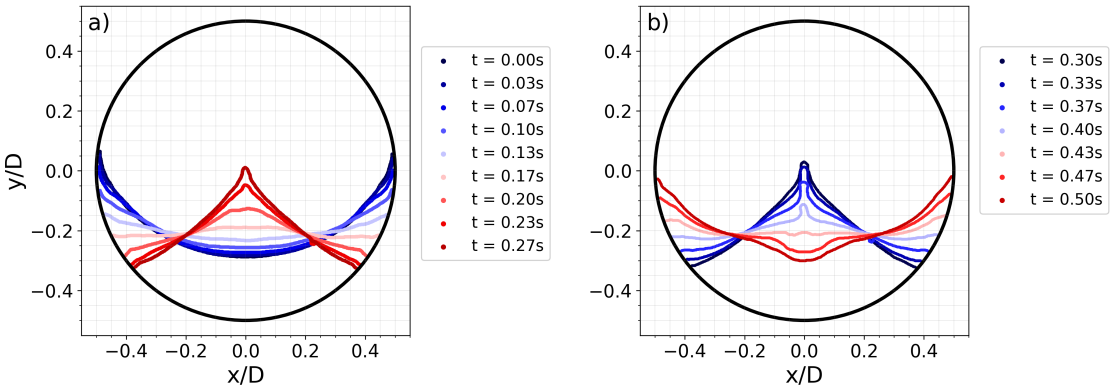

Figure 4: a) Increasing wave elevation b) Decreasing wave elevation

4 Conclusion

This abstract has described two dimensional sloshing in a circular tank. Forced vertical oscillating motion at principal parametric resonance has generated Faraday waves. Theoretical eigenfrequencies have been calculated using linear potential flow. These have been compared to experimental results of the steady state fluid. A soft spring nonlinear response is displayed, greater nonlinearities are present for larger forcing amplitudes and higher fill level ratios.

References

Canny, J. (1986), 'A computational approach to edge detection', *IEEE Transactions on pattern analysis and machine intelligence* (6), 679–698.

Colville, S. W., Ransley, E., Gambioli, F., Lee, Y. C. & Greaves, D. (2023), Fluid response of sloshing in a horizontal cylinder due to horizontal excitation, *in* 'ISOPE International Ocean and Polar Engineering Conference', ISOPE, pp. ISOPE–I.

Gambioli, F., Usach, R. A., Kirby, J., Wilson, T. & Behruzi, P. (2019), Experimental evaluation of fuel sloshing effects on wing dynamics, *in* 'Proceedings of the International Forum on Aeroelasticity and Structural Dynamics, Savannah, GA, USA', pp. 9–13.

Kumar, K. & Tuckerman, L. S. (1994), 'Parametric instability of the interface between two fluids', *Journal of Fluid Mechanics* **279**, 49–68.

McIver, P. (1989), 'Sloshing frequencies for cylindrical and spherical containers filled to an arbitrary depth', *Journal of Fluid Mechanics* **201**, 243–257.

Scolan, Y.-M. (2015), Some aspects of the eigenfrequency computation in a two-dimensional tank filled with two non miscible fluids, *in* '30th International Workshop on Water Waves and Floating Bodies, Bristol, UK', pp. 189–192.